Differentiation 107 (2019) 24–34

Contents lists available at ScienceDirect

Differentiation

journal homepage: www.elsevier.com/locate/diff

Osteogenic differentiation of human bone marrow-derived mesenchymal stem cells is enhanced by an aragonite scaffold

Csaba Matta[a,1], Csilla Szűcs-Somogyi[a,1], Elizaveta Kon[b,c], Dror Robinson[d], Tova Neufeld[e], Nir Altschuler[e], Agnes Berta[f], László Hangody[f], Zoltán Veréb[g], Róza Zákány[a,*]

[a] Department of Anatomy, Histology and Embryology, Faculty of Medicine, University of Debrecen, Nagyerdei krt 98, Debrecen, 4032, Hungary
[b] Department of Biomedical Sciences, Humanitas University, Via Rita Levi Montalcini 4, Rozzano, Milan, 20090, Italy
[c] Humanitas Clinical and Research Center, Via Alessandro Manzoni 56, Rozzano, Milan, 20089, Italy
[d] Orthopaedic Research & Foot and Ankle Unit, Rabin Medical Center, 39 Jabotinski St, Petah Tikva, 49100, Israel
[e] CartiHeal 2009 Ltd, Atir Yeda 17, Kfar Saba, 4464313, Israel
[f] Orthopaedic and Trauma Department, Uzsoki Hospital, Uzsoki ut 29, Budapest, 1145, Hungary
[g] Regenerative Medicine and Cellular Pharmacology Research Laboratory, Department of Dermatology and Allergology, Faculty of Medicine, University of Szeged, Koranyi fasor 6, Szeged, 6720, Hungary

ARTICLE INFO

Keywords:
Aragonite-based implant
Coralline scaffold
Osteogenesis
Bone marrow-derived mesenchymal stem cell
Energy dispersive x-ray spectroscopy
Agili-C

ABSTRACT

Bone graft substitutes and bone void fillers are predominantly used to treat bone defects and bone fusion in orthopaedic surgery. Some aragonite-based scaffolds of coralline exoskeleton origin exhibit osteoconductive properties and are described as useful bone repair scaffolds. The purpose of this study was to evaluate the *in vitro* osteogenic potential of the bone phase of a novel aragonite-based bi-phasic osteochondral scaffold (Agili-C™, CartiHeal Ltd.) using adult human bone marrow-derived mesenchymal stem cells (MSCs). Analyses were performed at several time intervals: 3, 7, 14, 21, 28 and 42 days post-seeding. Osteogenic differentiation was assessed by morphological characterisation using light microscopy after Alizarin red and von Kossa staining, and scanning electron microscopy. The transcript levels of alkaline phosphatase (*ALP*), runt-related transcription factor 2 (*RUNX2*), bone gamma-carboxyglutamate (*BGLAP*), osteonectin (*SPARC*) and osteopontin (*SPP1*) were determined by quantitative PCR. Proliferation was assessed by a thymidine incorporation assay and proliferating cell nuclear antigen (PCNA) immunocytochemistry. Our results demonstrate that the bone phase of the bi-phasic aragonite-based scaffold supports osteogenic differentiation and enhanced proliferation of bone marrow-derived MSCs at both the molecular and histological levels. The scaffold was colonized by differentiating MSCs, suggesting its suitability for incorporation into bone voids to accelerate bone healing, remodelling and regeneration. The mechanism of osteogenic differentiation involves scaffold surface modification with *de novo* production of calcium phosphate deposits, as revealed by energy dispersive spectroscopy (EDS) analyses. This novel coral-based scaffold may promote the rapid formation of high quality bone during the repair of osteochondral lesions.

Abbreviations: ALP, alkaline phosphatase; AR, Alizarin red; BGLAP, bone gamma-carboxyglutamate; BM-MSC, bone marrow-derived mesenchymal stem cell; CC, control culture; DCP, dicalcium phosphate anhydrous; ECM, extracellular matrix; EDS, energy dispersive X-ray spectroscopy; GAPDH, glyceraldehyde 3-phosphate dehydrogenase; H&E, haematoxylin and eosin; HMDS, hexamethyldisilazane; hMSC, human mesenchymal stem cell; HPRT1, hypoxanthine phosphoribosyl-transferase 1; MSCGM, Mesenchymal Stem Cells Growth Medium; PBS, phosphate buffered saline; PCNA, proliferating cell nuclear antigen; PPIA, peptidyl-prolyl isomerase-A (cyclophilin-A); RUNX2, runt-related transcription factor 2; SEC, scaffold-exposed culture; SEM, scanning electron microscopy; SPARC, secreted protein acidic rich in cysteine (osteonectin); SPP1, osteopontin; TGF, transforming growth factor

* Corresponding author. Department of Anatomy, Histology and Embryology, Faculty of Medicine, University of Debrecen, Nagyerdei krt 98, Debrecen, 4032, Hungary.

E-mail addresses: matta.csaba@med.unideb.hu (C. Matta), somogyics@anat.med.unideb.hu (C. Szűcs-Somogyi), Elizaveta.kon@humanitas.it (E. Kon), dror@cartiheal.com (D. Robinson), tova@cartiheal.com (T. Neufeld), nir@cartiheal.com (N. Altschuler), bertaagnes@hotmail.com (A. Berta), hangody.laszlo@hangody.hu (L. Hangody), vereb.zoltan@med.u-szeged.hu (Z. Veréb), roza@anat.med.unideb.hu (R. Zákány).

[1] These two authors equally contributed to the work.

https://doi.org/10.1016/j.diff.2019.05.002
Received 11 January 2019; Received in revised form 29 April 2019; Accepted 16 May 2019
Available online 22 May 2019

1. Introduction

The repair of joint lesions requires the reconstruction of both subchondral bone and articular cartilage. This challenging goal might be achieved by certain novel bi-phasic osteochondral scaffolds capable of stimulating both articular cartilage regeneration and subchondral bone repair. The intrinsic properties of the scaffold at the bony phase ought to be designed specifically to introduce structural, biological and biomechanical cues into the affected regions (Bowland et al., 2015). The optimal osteogenic scaffold should therefore allow bone repair in damaged areas by means of migration, proliferation and osteogenic differentiation of mesenchymal stem cells (MSCs) into the graft (Ciocca et al., 2015).

Multiple types of bony scaffolds are available, including calcium phosphate and calcium carbonate, and various combinations of both materials (Niu et al., 2015). Bone-like nanocomposite scaffolds made of sericin (a silk worm-protein) and hydroxyapatite crystals promote the osteogenic differentiation of human bone marrow-derived mesenchymal stem cells (BM-MSCs) (Yang et al., 2015a,b). Biomineralized hydroxyapatite small intestinal submucosa scaffolds were found to promote the osteogenic differentiation of MSCs in basal media without osteogenic supplements due to the presence of hydroxyapatite crystals in the scaffolds (Yang et al., 2015a,b). In a different approach, hydroxyapatite disks functionalised with a modular peptide formed of a hydroxyapatite-binding peptide motif and an osteogenic peptide motif were documented to induce the osteogenic differentiation of MSCs (Polini et al., 2014). To facilitate scaffold vascularisation and incorporation, a novel strategy involving a “smart matrix” composed of three key components (RGD-phage; porous bone-like biphasic calcium phosphate scaffold and MSCs) has been developed. Due to the presence of the RGD-phage nanofibres, the novel matrix can regulate endothelial cell migration and adhesion to induce vascularisation and simultaneously activate osteoblastic differentiation of MSCs, and thus induce both osteogenesis and angiogenesis *in vivo* (Wang et al., 2014).

Some of the scaffolds used clinically are coralline aragonite-based. The aragonite (a crystalline form of calcium carbonate) exoskeletons of certain coral species (marine invertebrates from the class *Anthozoa* of the phylum *Cnidaria*) are remarkably similar to human spongy bone with respect to its 3D structure, as well as macro- and micro-porosity and pore interconnections (Demers et al., 2002). These coralline calcium carbonate scaffolds have been shown to be biocompatible, osteoconductive, and biodegradable when used as bone grafts (Ripamonti, 2017); however, there is a controversy in the literature regarding the mechanism by which coral grafts transform into bone and three mechanisms are proposed.

The first hypothesis assumes that the coral graft is osteoinductive (Ripamonti et al., 2009); immature undifferentiated (stem) cells are recruited and the coral graft stimulates these cells to differentiate into pre-osteoblasts (Albrektsson and Johansson, 2001). A second mechanism has also been described by which the coral substrate acts merely as an osteoconductive material; osteoconduction is bone growth on a scaffold surface caused by the action of differentiated bone cells, which may include pre-existing pre-osteoblasts/osteoblasts activated by trauma, or cells recruited from mesenchymal cells by osteoinduction (Albrektsson and Johansson, 2001). Recently, certain bone substitute materials were reported to demonstrate a mixture of properties being both osteoinductive and osteoconductive (Conserva et al., 2013). A third mechanism, osteotransduction (Driessens et al., 1998), has been suggested for certain biomaterials consisting mostly of calcium phosphate that allow gradual reabsorption and replacement by newly formed functional bone tissue. Bone formation occurs by direct deposition of bone trabeculae on the scaffold material, which is similar to the clinically described mechanism of primary bone repair (Marsell and Einhorn, 2011).

The cell-free, bi-phasic aragonite-based scaffold (Agili-C™, CartiHeal Ltd.) used in this study is a biocompatible, resorbable material. The scaffold has been previously shown to be supportive of cartilage and bone repair in human patients (Scott, 2011). Agili-C™ is indicated for the treatment of osteochondral defects, in both inflammatory and non-degenerative joints. This scaffold is made of a composite material, which is intended to help restore the osteochondral unit through the *in situ* regeneration of both articular cartilage and its underlying subchondral bone, and to help reproduce the original structure and function of the affected tissues. The scaffold does not only effectively stimulate cartilage regeneration and repair *ex vivo* (Chubinskaya et al., 2018) but its suitability to facilitate osteochondral regeneration *in vivo* has been demonstrated in a caprine model (over a 6–12-month follow-up period), and also in humans (Kon et al., 2014a,b, 2015; Kon et al., 2016).

In the current study we examined the *in vitro* mechanisms induced by the bone phase of the Agili-C™ scaffold on the osteogenic differentiation of BM-MSCs cultured under differentiation-inducing conditions. BM-MSCs are multipotent and can differentiate into different cell lineages, such as adipocytes, myocytes, chondrocytes, or osteoblasts, depending on the composition and 3D organization of the extracellular matrix (ECM) and the combined effect of growth factors and other morphogens in their immediate environment (Pittenger et al., 1999).

We present data on enhanced osteogenesis of BM-MSCs seeded onto the scaffold and cultured under osteogenic conditions. The key observation of this study is that the phenomenon of *de novo* formation of calcium phosphate depositions on the aragonite scaffold surface *in vitro* by BM-MSCs has not been previously observed on the Agili-C™ scaffold. We show that the coral-derived aragonite scaffold has an ultrastructure and pore size similar to that of spongy bone, which favours osteoinduction, osteoconduction and potentially osteotransduction.

2. Methods

2.1. Experimental setup

The study was designed to evaluate the effect of the bone phase of Agili-C™, a coral-derived aragonite scaffold, on human BM-MSCs compared to cells grown in an osteogenic differentiation medium without scaffolds. The effect of the scaffold exposure was evaluated by proliferation assays, phenotypic assessment and gene expression assays to define scaffold-enhanced differentiation towards the osteogenic pathway. Scaffold-exposed cultures (SEC) were compared to control cultures (CC) grown in osteogenic differentiation medium (Thorpe et al., 2016).

2.2. Aragonite-based scaffold

The aragonite-based scaffold (Agili-C™, CartiHeal 2009 Ltd, Kfar Sava, Israel) is derived from the *Porites* species and characterised by interconnected pores with a mean pore diameter of 150 μm (range 100–300 μm) and ~50% porosity (Wu et al., 2009) (Fig. 1). Scaffold samples were provided by the manufacturer. Dimensions of the scaffold cylinders were as follows: Ø = 6 mm; height, 2 mm; the cylinders were taken from a serial production stock and contained the mineral phase only.

2.3. Cell cultures

Commercially available primary adult human BM-MSCs were used (Lonza Group Ltd., Basel, Switzerland). Cells were expanded in T75 cell culture flasks (Orange Scientifique, Braine-l’Alleud, Belgium) in hMSC Growth Medium (MSCGM™ Mesenchymal Stem Cell Growth Medium, Lonza). 1 mL aliquots (containing ~700,000 cells from passage 3) were frozen and stored in liquid nitrogen according to the manufacturer's instructions. For each experiment, one vial (always from passage 3) was thawed and cells were expanded in four T75 flasks until ~90% confluence (which took 10–14 days). Cells were detached using Trypsin/

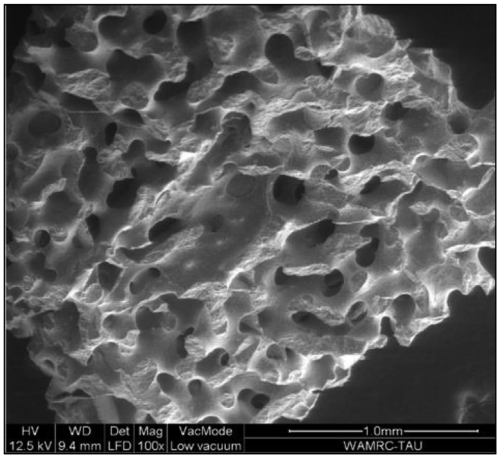

Fig. 1. SEM micrograph of the porous 3D structure of the aragonite scaffold used in this study. Scale bar, 1 mm.

EDTA for MSC (Lonza), centrifuged at 600 × *g* for 5 min, and re-suspended. The cell suspension (20,000 cells/cm^2) was seeded onto scaffolds placed in 24-well cell-culture plates (Orange Scientifique) with round cover glasses (Ø = 10 mm; thickness = No.1; Menzel-Gläser, Menzel GmbH, Braunschweig, Germany). Controls were seeded directly onto coverslips without the scaffolds in a single droplet. Following a 2 h adherence period cultures were fed with growth medium (MSCGM™). At 24 h post seeding, medium was changed to osteogenic differentiation medium (hMSC Osteogenic Differentiation BulletKit™ Medium, Lonza). Cultures on various days were subject to analyses. For histological staining procedures, cells attached to the coverslips in the vicinity of the scaffold were used, due to the fact that cells growing inside the scaffolds would have been impossible to analyse using light microscopy.

2.4. Phenotypic confirmation of bone marrow-derived MSCs

Flow cytometry was used for phenotyping the adult bone marrow-derived MSCs, to rule out de-differentiation. Cells were analysed from passage 3. The following haematopoietic and mesenchymal stem cell surface markers were assessed: CD29/Integrin β1, CD34, CD47, CD73, CD90/Thy-1 (Biolegend, San Diego, CA, USA); CD45, CD146/Melanoma cell adhesion molecule (MCAM), CD117/c-kit (R&D Systems, Minneapolis, MN, USA) and CD105/Endoglin (BD Biosciences, San Jose, CA, USA). Cells cultured in a monolayer were harvested with 0.025% trypsin/EDTA, washed twice with Fluorescence-Activated Cell Sorting (FACS) buffer (0.5% bovine serum albumin and 0.05% Na-azide dissolved in PBS), incubated with the selected antibodies (according to the manufacturer's protocol) on ice for 30 min, then washed with FACS buffer and measured by a FACSCalibur flow cytometer (BD Biosciences, Franklin Lakes, NJ, USA). Data were analysed using FlowJo LLC Data Analysis Software (Ashland, OR, USA). Results are expressed as means of positive cells (%).

2.5. Histological procedures

1. Investigation of cellular morphology with conventional haematoxylin and eosin (H&E) staining

Cultures were maintained up to 42 days and assessments were carried out on days 14, 28, 35 and 42 post-seeding. In brief, cultures were washed with phosphate buffered saline (PBS) and fixed with a 4:1 mixture of absolute ethanol and 4% formaldehyde (Sigma-Aldrich, St. Louis, MO, USA). After rehydration in a descending series of ethanol, cells were stained with Gill's haematoxylin No. 2 and eosin Y (1% aqueous solution; Bio Optica Milano S.p.A., Italy). Cultures were first immersed in haematoxylin for 20 s, rinsed in running tap water for 5 min, and after washing in distilled water, eosin was applied for 2 min. Eosin was removed and cultures were dehydrated in ascending series of ethanol, and after a final wash in xylene, colonies were mounted onto glass slides using DPX mounting medium (Sigma-Aldrich). Photomicrographs of the cultures were taken using an Olympus DP72 camera on a Nikon Eclipse E800 microscope (Nikon Corporation, Tokyo, Japan), and images were prepared using cellSens 1.5 software (Olympus, Japan).

2. Assessment of matrix mineralisation by Alizarin Red S staining

To demonstrate the extent of matrix calcification the cultures were fixed with the same fixative as above on various days of culturing, then stained for 2 min with 2% (w/v) Alizarin Red S (Sigma-Aldrich) dissolved in distilled water and pH was adjusted with 10% ammonium hydroxide to pH 4.2. Excess dye was removed, then the coverslips were dipped into acetone (20 times) for dehydration, and then into acetone–xylene (1:1) mixture (20 times). Coverslips were finally mounted onto glass slides using DPX mounting medium (Sigma-Aldrich). Photomicrographs of the cultures were taken as described above.

3. Assessment of matrix mineralisation by von Kossa staining

As an alternative method, matrix mineralisation was also assessed by von Kossa staining. Formalin and ethanol-fixed cultures were incubated with 1% silver nitrate and placed under UV light for 10 min, rinsed in distilled water, and unreacted silver was removed with 5% sodium thiosulphate for 5 min. After rinsing in distilled water, specimens were counterstained with 0.1% nuclear fast red solution for 5 min. Finally, samples were dehydrated through graded ethanol, and mounted using DPX mounting medium. Photomicrographs of the cultures were taken as described above.

2.6. Cell proliferation assays

Radioactive thymidine incorporation assay was performed on culturing days 3, 7, 14, and 21 in 3 independent experiments. Cell culture medium containing 1 μCi/mL ^{3}H-thymidine (185 GBq/mM ^{3}H-thymidine, Amersham Biosciences, GE Healthcare UK Ltd, Little Chalfont, UK) was added to the wells for 48 h. After washing with PBS, proteins were precipitated with ice-cold 5% trichloroacetic acid, and washed with PBS again. Then, trypsin-digested cell lysates were transferred to special, opaque 96-well microtiter plates (Wallac, PerkinElmer Life and Analytical Sciences, Shelton, CT, USA). Samples were air-dried for 2 weeks at room temperature and radioactivity was counted by a Chameleon liquid scintillation counter (Hidex Oy, Turku, Finland).

Proliferating cell nuclear antigen (PCNA) immunocytochemistry was used to visualise proliferating cell topology within the cultures in 3 independent experiments. 14-day-old scaffold (SEC) and control cultures (CC) were used. Samples were fixed with a 4:1 mixture of absolute ethanol and 40% formalin for 30 min, followed by permeabilization with ice-cold methanol for 10 min at − 20 °C. After washing the cultures with PBS, specific binding sites were blocked for 1 h in PBS containing 5% normal goat serum and 0.3% Triton X-100. Thereafter, samples were incubated with the PCNA primary antibody (Cell Signaling Technology Inc, Davers, MA, USA) at a dilution of 1:2,400 in blocking buffer overnight at 4 °C. After washing, the secondary antibody (Alexa Fluor® 555 Goat anti-mouse IgG; A21422; Life Technologies, Carlsbad, CA, USA) was applied at a dilution of 1:1,500 in PBS for 1 h at room temperature. Subsequently, specimens were washed with PBS and covered with anti-fade medium containing DAPI (Vectashield mounting medium; Vector Laboratories, Peterborough, England). Photomicrographs were taken by an Olympus DP72 camera on a Nikon Eclipse E800 microscope (Nikon Corporation). Images were acquired using cellSens Entry 1.5 software (Olympus). Proliferating cells were

counted using the Automatic Nuclei Counter plug-in for ImageJ (downloaded from https://imagej.nih.gov/ij/plugins/itcn.html) following the analysis of 3–3 images taken from each experiment.

2.7. Sample preparation for scanning electron microscope (SEM) analysis

Aragonite-based scaffolds removed from cell cultures on various days of culturing were fixed with a 4:1 mixture of absolute ethanol and 4% formaldehyde. After 30 min, the fixative was washed with 80% ethanol. Samples were then rinsed and stored in 70% ethanol at −20 °C. 3 successive washes were performed with increasing series of ethanol (90%, 95% and 100%) for 10 min. The scaffolds were dried by successive washes with 0.2 mL hexamethyldisilazane (HMDS) at concentrations of 33%, 50%, and 67% for 1 min each. A last wash was performed with 0.2 mL of 100% HMDS 3 × for 1 min. The solution was removed and samples were left to dry in the chemical hood overnight.

2.8. Scanning electron microscopy

SEM (JEOL Ltd., Tokyo, Japan - JSM 35 CF) analyses were performed at Ariel University, Israel. Each specimen was glued to a mounting stab, coated with gold and observed at 15–20 keV. Elemental analysis (SEM-EDS) was performed using the same instrumentation.

2.9. Gene expression analyses using RT-qPCR

Relative gene expression levels of alkaline phosphatase (*ALP*), runt-related transcription factor 2 (*RUNX2*), bone gamma-carboxyglutamate (*BGLAP*), osteonectin (secreted protein, acidic, rich in cysteine or *SPARC*) and osteopontin (*SPP1*) genes were determined by RT-qPCR measurements using an Applied Biosystems™ QuantStudio™ 12K Flex Real-Time PCR System (Life Technologies, CA, USA). The Universal Probe Library (UPL) Assay Design Center (Roche, Bazel, Switzerland) was used to design specific primer pairs. The sequences used for amplifications were as follows: *ALP* (FW: 5′– TCA CTC TCC GAG ATG GTG GT –3′, Rev: 5′–GTG CCC GTG GTC AAT TCT–3′, UPL: #12); *BGLAP* (FW: 5′–GAA GAG ACC CAG GCG CTA C–3′, Rev: 5′–CTC ACA CAC CTC CCT CCT G–3′, UPL: #45); *RUNX2* (FW: 5′–GGC GCA TTT CAG ATG ATG A–3′, Rev: 5′–GCC CAG TTC TGA AGC ACC T–3′, UPL: #87); *SPARC* (FW: 5′–TTC CCT GTA CAC TGG CAG TTC–3′, Rev: 5′–AAT GCT CCA TGG GGA TGA–3′, UPL: #36); *SPP1* expression was measured using IDT PrimeTime assay (ID: Hs.PT.58.19252426). For data normalization the following three reference genes were tested: glyceraldehyde-3-phosphate dehydrogenase (*GAPDH*), assay code: Hs99999905_m1; peptidyl-prolyl isomerase A (*PPIA*), assay code: Hs99999904_m1; and hypoxanthine phosphoribosyl-transferase 1 (*HPRT1*), assay code: Hs03929098_m1 (Life Technologies).

On various days of culturing, cell cultures (a total of 3 per group and per culturing day) were dissolved in Trizol (Applied Biosystems, Foster City, CA, USA), total RNA was harvested in RNase-free water, and stored at −80 °C. First strand cDNA was generated from 1 µg total RNA using the High Capacity cDNA Reverse Transcription Kit (Life Technologies). RT-qPCR measurements were performed in an ABI Prism 7900 Real-Time PCR System (Life Technologies) in 96-well plates using 2 × TaqMan Gene Expression Master Mix (Life Technologies), with the following thermal cycling conditions: enzyme activation at 95 °C for 1 min, followed by 40 cycles of denaturation at 95 °C for 12 s and annealing/extension at 60 °C for 45 s.

To find the best normalising gene, standard deviations of gene expression levels of reference genes were calculated between samples, and *PPIA* was found to show the lowest standard deviation values. Therefore, *PPIA* expression was used to determine relative gene expression levels, which were calculated by the comparative Ct method. In the comparative or ΔΔCt method of qPCR data analysis, the Ct values obtained from two different experimental RNA samples are directly normalized to the reference gene (*PPIA*) and then compared. Hierarchical cluster analysis based on the relative expression levels of selected genes was performed by the R software package.

2.10. Statistical analysis

All data are representative of at least three independent experiments. Where applicable, data are expressed as mean ± SD. Data was tested for normality using the Kolmogorov-Smirnov test and then statistical analysis was performed by two-way ANOVA using the all-pairwise multiple comparison procedure (Holm-Sidak method). Statistical analyses were performed using SigmaStat version 3.5. The level of significance was set as follows: $*P < 0.05$; $**P < 0.01$.

3. Results

3.1. Validation of the mesenchymal stem cell phenotype

To rule out potential phenotypic changes during culture, cells retrieved from frozen aliquots were immunophenotypically evaluated. Cells cultured in growth medium maintained the expression of cell

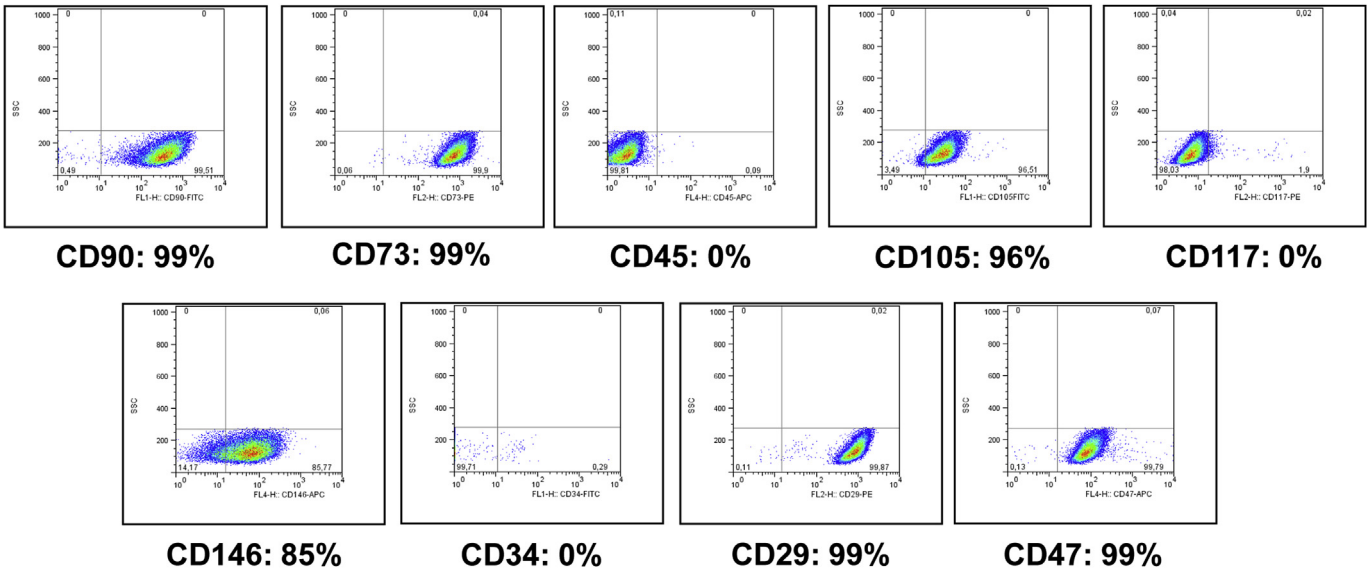

Fig. 2. CD marker expression analysis and immunophenotypic characterisation of hMSCs expanded in growth medium using FACS.

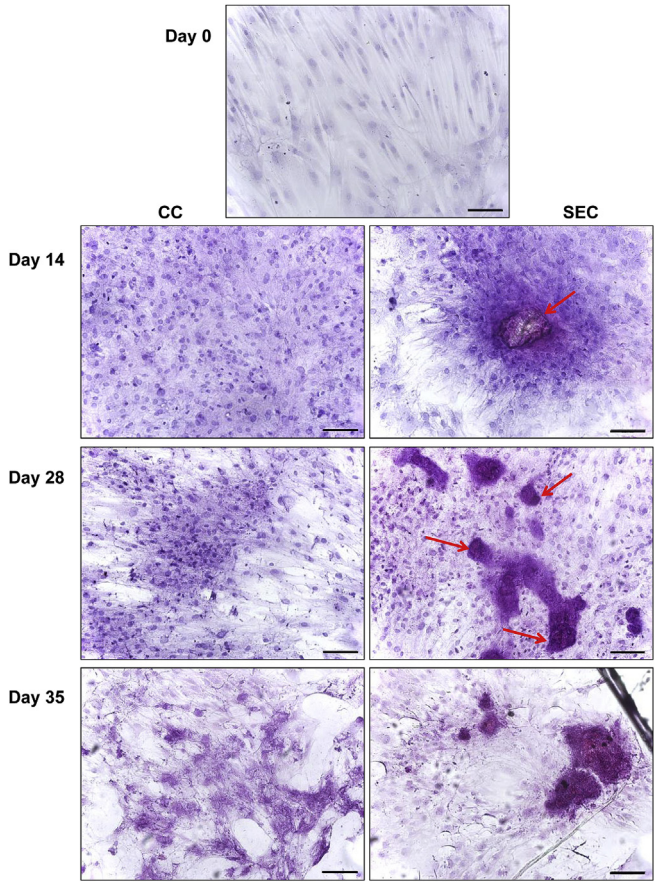

Fig. 3. Changes in cell morphology of hMSCs cultured in osteogenic medium in the presence and absence of aragonite scaffold, for 14, 28 and 35 days (H&E staining). CC-Control Culture (left), SEC-Scaffold Exposed Culture (right). Original magnification, 20×; scale bar, 100 μm for all images. Arrows indicate small fragments of the scaffold and the increased density of cells around them.

surface markers characteristic to hMSC; they were found to be positive for CD90, CD73, CD105, CD146, CD47 and CD29; and negative for CD45, CD117 and CD34 (Dominici et al., 2006) (Fig. 2). Expressions of CD105, CD73 and CD90 are characteristic for MSCs, lack of CD45 proved the absence of leukocytes, and no staining for CD117 and CD34 confirmed the absence of haemopoietic stem cells and endothelial cells from the cell culture. These results confirmed that the human cells used in the study fulfilled the minimal criteria of multipotent MSCs, a property that was preserved during the entire expansion period.

3.2. Cell culture morphology visualized by H&E staining

On day 0 the cells exhibited typical mesenchymal morphology forming a monolayer culture composed of spindle-shaped cells (Fig. 3). Differences in cellular morphology were noted between the SEC and the CC groups at later time points (e.g. on day 14 as shown in Fig. 3). A spatial zonation phenomenon occurred in the SEC group depending on the proximity to the scaffold material starting from day 14. Cells in direct contact with the scaffold and/or its fragments attached to the scaffold surface with numerous cellular podia. They had large, oval-shaped nuclei and a rather basophilic cytoplasm, indicating active protein synthesis. The cells located in the more peripheral zone (average zone width about 150 μm) were cuboidal and formed multi-layers around the scaffold. The morphology of the latter cell population also demonstrated features of active protein synthesis. Farther away from the scaffold the morphology of the SEC cultures was quite similar to the CC cultures with spindle shaped monolayer cells predominating.

Both CC and SEC cultures exhibited a temporal series of sequential

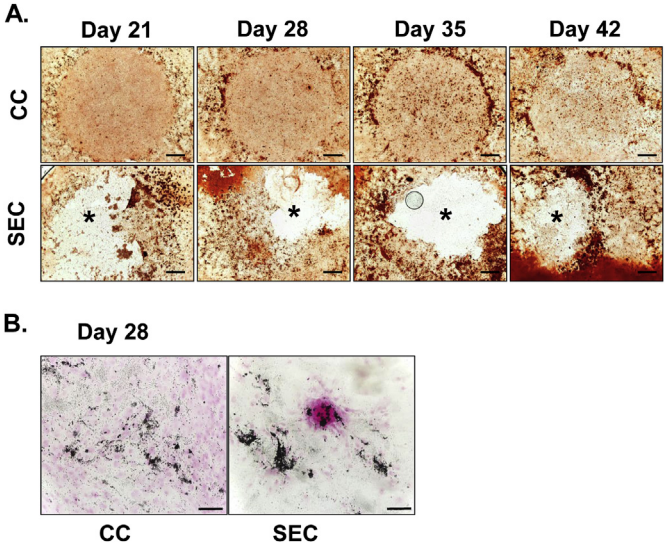

Fig. 4. A. Calcified matrix depositions in hMSCs cultured in osteogenic medium for 21, 28, 35 and 42 days. Calcified matrix depositions were visualized with AR staining (reddish-brown areas). The positions of the implants after their removal (see SEC row) are labelled with asterisks (*). Images are representative of four independent experiments. Scale bars, 1 mm for all images. The circular contours in the control (CC) row represent the edges of droplets in which the cells were seeded on day 0. **B.** hMSCs cultured in osteogenic medium for 28 days. Calcium and phosphate salt-containing deposits were visualized with von Kossa staining on culturing day 28. Mineralised matrix depositions are visible as black-grey precipitations. Specimens were background stained using nuclear fast red. Original magnification, 20×; scale bars, 100 μm for both images. (For interpretation of the references to colour in this figure legend, the reader is referred to the Web version of this article.)

morphological stages. In SEC cultures, during the first stage (by day 14), cells became thicker and shorter but still spindle shaped. Their cytoplasm was more basophilic than prior to osteogenic induction, and possessed a euchromatic, large, oval shaped nucleus. At a later stage (at 28 days), the majority of CC cells became larger and changed their morphology to cuboidal or polygonal. Most of the cells were characterised by large spherical nuclei. Later, multilayer formation occurred mainly in the SEC cultures with the appearance of small basophilic nodules that gradually coalesced (in CC cultures complete coalescence was not achieved during the 42-day-long culture period). This stage was also characterised by a robust production of ECM by the cells. The SEC group cultures demonstrated an accelerated differentiation process as compared to the CC group.

3.3. Culture mineralisation

Alizarin Red (AR) staining was used to demonstrate the presence of mineralised (calcified) matrix areas in BM-MSC cultures. There was a massive mineralisation in SEC cultures, whilst only weak staining was observed in CC cultures by day 21 (Fig. 4A). The deposition of inorganic calcium salts was the most prominent directly surrounding the scaffolds and a more heavily AR-positive mineralised area was visible in the peripheral region of cultures with the aragonite scaffolds. Control cultures showed little increase in AR-positivity over time (primarily at the edge of the droplet culture), while those with the scaffolds exhibited a prominently increased calcification by day 42. Stronger von Kossa staining also indicated a more intense biomineralisation in the SEC cultures than in CC cultures (Fig. 4B).

3.4. SEM analysis

To investigate cell adhesion on the scaffold, as well as to better

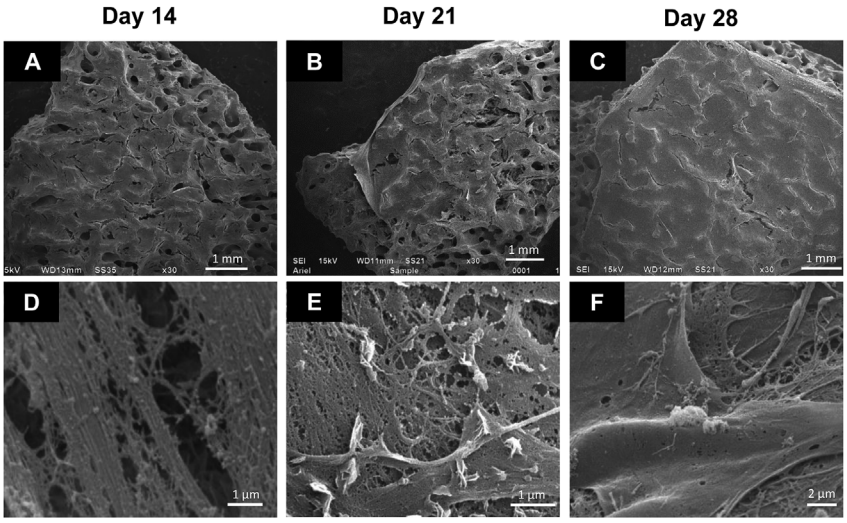

Fig. 5. SEM images of cell layer growth on aragonite scaffolds after 14, 21 and 28 days. **A** and **D.** Day 14 showing incomplete cell layer coverage. **B** and **E.** Day 21 showing almost complete cell layer coverage. **C** and **F.** Day 28 showing complete and complex cell layer formation. For images **A, B** and **C**, original magnification was 30 × (scale bar, 1 mm). For **D, E** and **F**, original magnification was 10,000 × (scale bar, 1 or 2 µm as shown).

characterise the newly formed ECM secreted by the differentiating MSCs, SEM analyses were performed. hMSCs adhered and spread on the surface of the scaffold by forming a thick layer of cells covering the pores of the scaffold as early as day 14 (Fig. 5). The complexity of the tissue-like multilayer culture was observed to grow with time until the coral surface was almost completely covered by day 28.

Scanning the scaffold surface at certain locations and at higher magnifications revealed the presence of a microstructure deposit exhibiting a unique morphology, not typical of natural aragonite (Fig. 6; day 0 representing the typical aragonite surface, compared to days 14–28). This deposit exhibited increased complexity over time, beginning as a rather flat surface at day 14 and culminating in a rough hill-like topology at day 28 (Fig. 6A). Energy dispersive spectroscopy (EDS) analysis of the deposit identified the presence of phosphate 14 days post-seeding (Fig. 6B). In the natural aragonite, no phosphate peak was observed (Fig. 6B inset). The morphology of these deposits at this time point was similar to the typical calcium phosphate microstructures (Kazemzadeh-Narbat et al., 2010).

SEM analysis revealed cells adhering to the deposited calcium phosphate layer as well as cells covered by spherical deposits (Fig. 7). These were shown by EDS to be calcium phosphate and morphologically similar to typical hydroxyapatite bundles (Scaglione et al., 2008). The surface deposition and substitution of the natural aragonite scaffold by phosphate into a material which can be similar to hydroxyapatite present in the inorganic phase of bone can make these scaffolds an ideal cell adhesion material.

3.5. Proliferation rate

The proliferation rate of the hMSCs was assessed by incubating the cultures with ^{3}H-thymidine-containing osteogenic differentiation medium for 48 h. Cells in SEC cultures exhibited a significantly increased proliferation rate on days 3, 7 and 14, but no significant difference could be detected by day 21 relative to control (Fig. 8A).

Given the detected increase in proliferation in the SEC population, we wanted to rule out a potential artifact caused by the increased culture area (as the scaffolds offer a larger 3D surface for the cells to expand on). Therefore, to examine the spatial distribution of proliferating cells, PCNA immunocytochemistry was performed on 14-day-old cultures. In dividing cells, PCNA was clearly localised in the nucleus. Cells in the SEC culture located close to the scaffold or its fragments on the coverslip displayed higher PCNA levels compared to CC cultures or to cells of the SEC cultures located at a distance greater than ~150 µm from the scaffold (Fig. 8B). Cell counting revealed an approx. three-fold increase in the number of dividing cells in the SEC cultures (14.17% ± 6.83 in CC vs. 49.08% ± 22.42 in SEC). These findings clearly indicate a stimulating effect of the scaffold on the proliferation rate of hMSCs.

3.6. Expression of osteogenic marker genes in the presence of the Agili-C™ scaffold

The relative mRNA expression levels of the osteogenic marker genes alkaline phosphatase (*ALP*), bone gamma-carboxyglutamate (*BGLAP*; osteocalcin), runt-related transcription factor 2 (*RUNX2*), osteonectin (*SPARC*) and osteopontin (*SPP1*) were monitored at an early (7-day) and a late (28-day) time point using RT-qPCR (Fig. 9).

RUNX2 was upregulated on day 7 in the SEC culture compared to the CC cultures. It was downregulated by day 28 in the SEC culture, while expression was constant at both time points in CC cultures. Alkaline phosphatase expression was similar in SEC and CC cultures at both time points. Osteopontin mRNA (*SSP1*) was upregulated in control cultures by day 28, and peaked in the SEC culture on day 28 (7.9-fold increase, $^{*}P = 0.004$). In both cultures, *BGLAP* expression showed a strong downregulation by day 28 compared to day 7. *SPARC* transcript levels in SEC culture exhibited a similar downregulation pattern over time to those of *BGLAP* (4.36-fold change, $^{*}P = 0.007$); however, it maintained a steady expression in the control CC culture.

Hierarchical clustering of gene transcripts revealed groups based on overall gene expression patterns of the studied marker genes. The clustering clearly separated the 7-day control cultures, and showed that the 7-day SEC cultures were more related to the 28-day cultures (both CC and SEC), implicating a more advanced osteogenic gene expression pattern caused by the scaffold even at this early stage (Fig. 9F).

4. Discussion

Tissue engineering requires either the introduction of cells capable of reconstructing the tissue (Mesallati et al., 2015) or the recruitment of such cells either from local or systemic sources (Fermor et al., 2015). Based on their favourable structural nanoscale characteristics and their osteoconductive properties, coral-based aragonite constructs are an emerging bone graft substitute and bone void filler in orthopaedic surgery, cranial and maxillofacial reconstruction, spine fusions and periodontal surgery. Following implantation, aragonite-based biomaterials are gradually reabsorbed and replaced by the newly generated bone tissue (Chiroff et al., 1975; Guillemin et al., 1987; Ohgushi et al., 1992; Olah and Borbas, 2008). In order to better understand the mechanism of osteoinduction by the coral scaffolds, several *in vitro* and *in vivo* studies have been performed. MSC-seeded biodegradable coralline

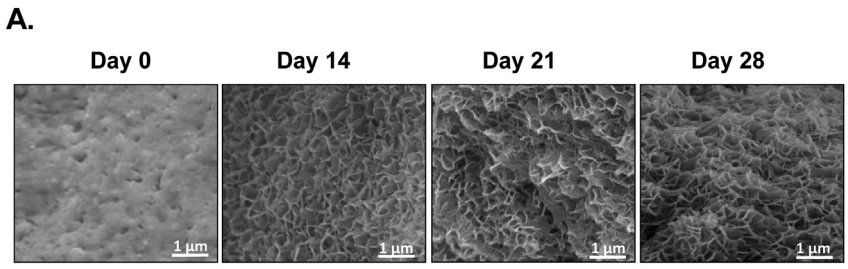

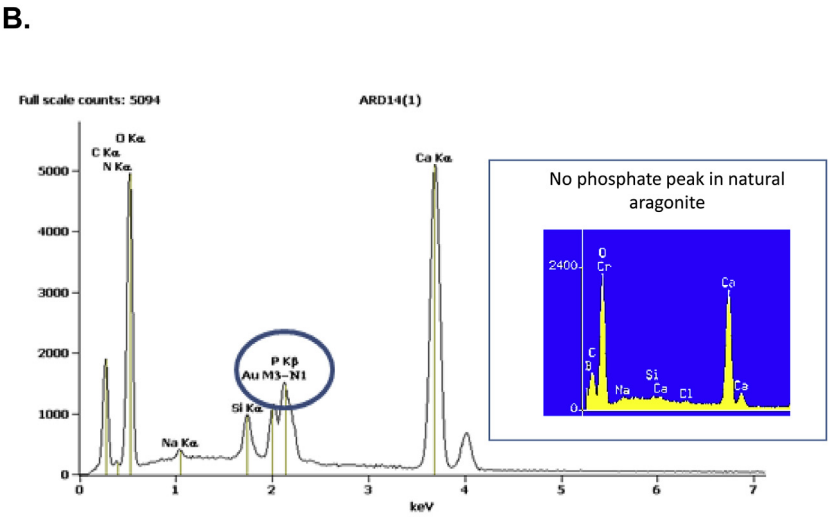

Element Line	Weight %	Weight % Error	Atom %	Atom % Error
C K	6.77	± 0.09	11.19	± 0.14
N K	3.81	± 0.56	5.40	± 0.79
O K	51.24	± 0.44	63.52	± 0.55
Na K	0.60	± 0.04	0.52	± 0.03
Si K	2.11	± 0.04	1.49	± 0.03
P K	2.31	± 0.12	1.48	± 0.07
Ca K	33.15	± 0.22	16.41	± 0.11
Total	**100.00**		**100.00**	

Fig. 6. A. SEM images showing the formation of the complexed microstructure deposits over time (0, 14, 21, and 28 days) exhibiting a calcium phosphate-like unique morphology. Day 0 represents the typical surface morphology of natural aragonite scaffold. Scale bar, 1 µm for all images. **B.** SEM-EDS elemental analysis of the deposit layer formed on the aragonite surface area 14 days post-seeding. The phosphate peak (2.31% weight) is marked with a circle. **Insert** – EDS spectrum of natural aragonite showing absence of phosphate.

hydroxyapatite/calcium carbonate composite scaffolds implanted into an immunodeficient mouse model or into human patients as void fillers appeared to be an excellent biodegradable *in vivo* bone graft material as they biointegrate with the host and induce osteoconduction (Harris and Cooper, 2004; Fu et al., 2013). The *in vitro* osteogenic capacity of coral-based hydroxyapatite and aragonite scaffolds with MSCs of varied origins has been evaluated by an array of SEM, fluorescent microscopic and transcriptional analyses (Al-Salihi and Samsudin, 2004; Mygind et al., 2007; Figueroa et al., 2011; Puvaneswary et al., 2013), but none of these studies used such a wide set of methodology that is presented in this work. Also, to the best of our knowledge, a comprehensive study on the molecular background of the osteogenic cell differentiation potential of the Agili-C™ scaffold using BM-MSCs has not yet been carried out.

The current *in vitro* study aimed to elucidate the mechanism of action underlying bone regeneration induced by the bone phase of the Agili-C™ aragonite-based scaffold. We first characterised the morphology (porosity and pore size) of the scaffold using SEM analysis, which revealed that the pores in the scaffold were interconnected, the mean pore diameter was 150 µm (range 100–300 µm) and porosity was ~50%; these features were remarkably similar to bone grafts (Puvaneswary et al., 2013). According to the basic assumption that the cells that first enter the scaffold upon implantation are from the bone marrow, we used commercially available primary adult human bone marrow-derived MSCs for this work, which have the potential to differentiate towards the osteogenic lineage (Pittenger et al., 1999).

Osteotransduction, the process whereby after implantation into bone *in vivo*, the scaffold material is transformed into new bone tissue, is known to occur to a limited extent in calcium phosphate bone cements (Driessens et al., 1998) due to direct cell attachment to the surface. The degree of osteotransduction may depend on the availability of dicalcium phosphate anhydrous (DCP) and $CaCO_3$ in the cement and can be significantly (up to 50%) enhanced with the addition of TGF-β1 (Blom et al., 2001). As the scaffold used in this study is composed of 98% calcium carbonate, a part of the surface should be transformed into calcium phosphate for enhanced biocompatibility. Our SEM analyses demonstrated the presence of newly formed calcium phosphate deposition on the surface of the aragonite-based scaffolds (either as a result of osteoconduction or osteotransduction). These deposits grew in complexity with the passage of time and SEM analysis demonstrated direct cell adherence to this newly formed surface layer.

Moreover, the presence of the coralline scaffold enhanced the proliferation of MSCs and the formation of multilayer cultures on its surface. The proliferation rate was higher in the SEC cultures as compared to CC cultures. At the same time, based on histological and gene

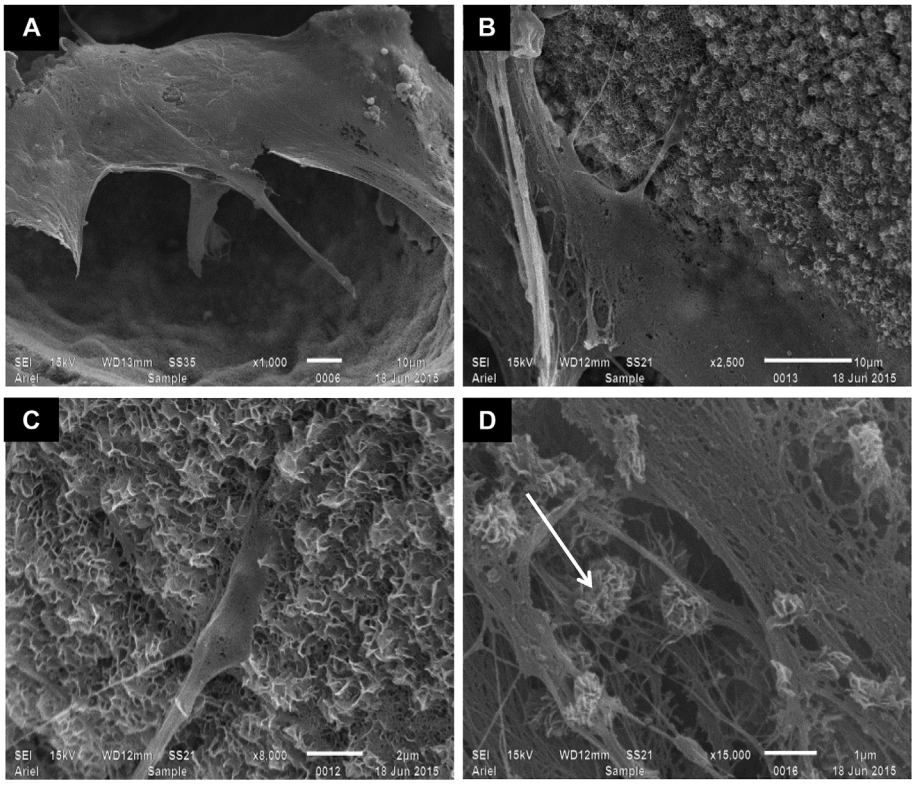

Fig. 7. Cell adherence to the calcium phosphate deposited layer formed on the aragonite scaffold. **A.** A cell sending processes to the coral surface (original magnification, 1,000×; scale bar, 10 µm). **B–C.** Higher magnification SEM images (original magnifications, **B –** 2,500×, **C** – 8,000×; scale bars, **B –** 10 µm, **C –** 2 µm) showing cell adherence to the deposited calcium phosphate layer. **D.** Spherical deposits (arrow) appeared as early as culturing day 14 on the aragonite scaffold (original magnification, 15,000×; scale bar, 1 µm).

expression analyses, osteoblastic differentiation appeared to progress more rapidly in the scaffold-exposed culture compared with stem cell cultures grown without scaffolds in osteogenic differentiation medium. The differentiation sequence was similar in both cultures, but all stages took place earlier in the presence of the scaffolds.

The mRNA levels of several classic osteogenic genes such as *RUNX2*, *ALP* and *SPP1* were enhanced by the presence of the scaffold. *RUNX2* is an essential transcriptional factor for the activation of osteoblast-associated genes, and is therefore an important early indicator of osteoblast differentiation and bone formation (Ducy et al., 1997). *RUNX2* directly activates the transcription of genes such as osteocalcin *(BGLAP)*, osteopontin *(SPP1)*, collagen type I, bone sialoprotein, or alkaline phosphatase *(ALP)*. A 4-fold upregulation was reported by Birk and colleagues just 1 h after cell seeding in 3T3F442A preadipocytes seeded onto coralline scaffolds (Birk et al., 2006). The current study did not examine such early time points. The detected *RUNX2* expression pattern in scaffold-exposed cells (SEC) was more pronounced than that of controls (CC) by day 7 of culturing, and declined by day 28. *RUNX2* is typically downregulated in 3 or 4-week-old cultures (Wu et al., 2014). This downregulation is an important indicator of matrix maturation and mineralisation. The lack of downregulation observed in the CC cultures probably indicates a delay or lack of matrix mineralisation. Indeed, von Kossa staining indicated that the extent of mineralisation was more advanced in the SEC cultures compared with CC cultures. Similar results were observed with AR staining, in which the staining in the CC cultures reached a plateau on day 28 whilst it has steadily progressed in the SEC cultures.

The mRNA expression profiles of genes that code for other non-collagenous proteins with important roles in osteogenesis, i.e. osteopontin (*SPP1*), osteonectin (*SPARC*) and osteocalcin (*BGLAP*) also confirmed the osteogenesis-promoting effect of the aragonite scaffolds on BM-MSCs. *SPP1* codes for one of the most predominant non-collagenous proteins in bone ECM produced by osteoblasts, and it also promotes cell adhesion to the bone surface (Sodek et al., 2000). We detected an upregulation of *SPP1* 28 days post-seeding in the presence of the scaffolds compared to day 7, which correlates well with data available in the literature (Beck et al., 2000; Foo et al., 2008). The expression of *SPARC*, a non-structural glycoprotein secreted by osteoblasts was massively decreased by day 28 in SEC cultures compared to CC cultures. This protein binds calcium in bone, has an affinity for collagen and is also involved in cell-matrix interactions (Ram et al., 2015). Osteonectin expression was found to be strongly upregulated in a coral graft culture system during osteogenic differentiation of mouse MSCs (Puvaneswary et al., 2013). However, given that *SPARC* is more strongly expressed during the early stages of osteogenesis (i.e. during the proliferative and matrix deposition periods) (Beck et al., 2000; Kulterer et al., 2007), our results may suggest that in the presence of the scaffold, osteogenic differentiation was accelerated relative to the control cultures. As cells progressed towards the later stages of osteogenic differentiation, SPARC was already downregulated by day 28.

A low expression of *BGLAP* (osteocalcin) can be explained by the fact that it is produced mainly by mature osteoblasts during the mineralisation phase, although its transcripts can also be detected during the earlier stages of osteogenesis, such as proliferation (Beck et al., 2000; Zoch et al., 2016). Nonetheless, a very similar osteocalcin mRNA expression pattern was observed during the osteogenic induction of periodontal ligament-derived cells (Choi et al., 2011).

Alkaline phosphatase (*ALP*), an important marker for bone matrix mineralisation and is therefore a widely used marker for *in vitro* osteoblastic phenotype characterisation (Fedde, 1992). Its expression remained constant in the SEC cultures.

Osteoblastogenesis and *de novo* bone formation are defined by four major phases: lineage commitment, proliferative expansion, synthesis of primary bone ECM (osteoid), and mineralisation (Javed et al., 2010). In many cell culture systems, osteoblastic proliferation takes place at the expense of maturation. Our results suggest that the Agili-C™ scaffold in SEC cultures may uniquely stimulate both proliferation and differentiation compared to the CC cultures. In our study, the proliferation rate in SEC cultures was higher than in CC cultures up to day 14, when it was found to be more than 3 times higher in the presence of the scaffold compared to the CC cultures. Proliferation rate returned to control levels by the end of the 21 days long culturing period, which

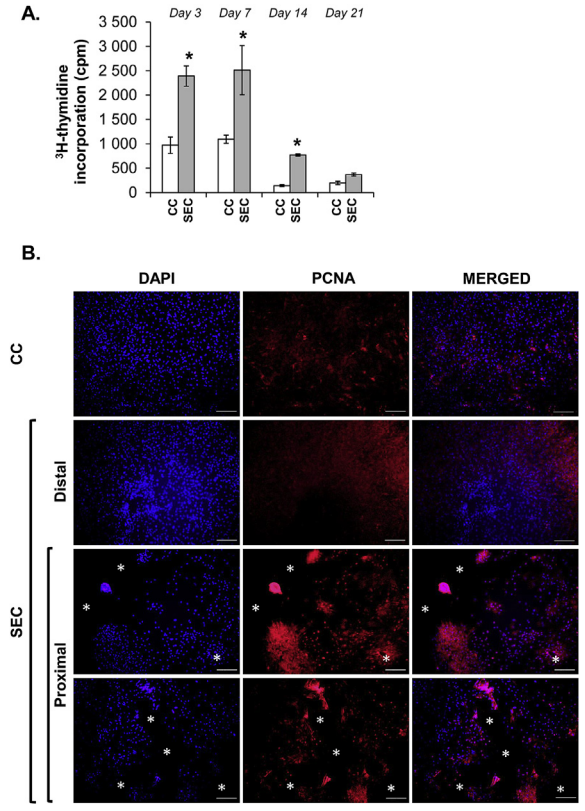

Fig. 8. A. Proliferation rates detected by ^{3}H-thymidine incorporation of CC and SEC cultures maintained in osteogenic medium for 3, 7, 14 and 21 days. Statistically significant proliferation rates were detected on days 3, 7 and 14 compared to control cultures (CC) ($n = 3$; $^{*}P < 0.05$). **B.** Proliferating Cell Nuclear Antigen (PCNA) immunocytochemistry of CC and SEC cultures. The number of dividing cells is higher in the proximal zone of the scaffold or its fragments (SEC, position of the removed implant fragments were labelled by asterisks). Representative photomicrographs out of three independent experiments are shown. Original magnification, 10×. Scale bar, 200 μm for all images. **CC**-Control culture; **SEC**-Scaffold Exposed Culture.

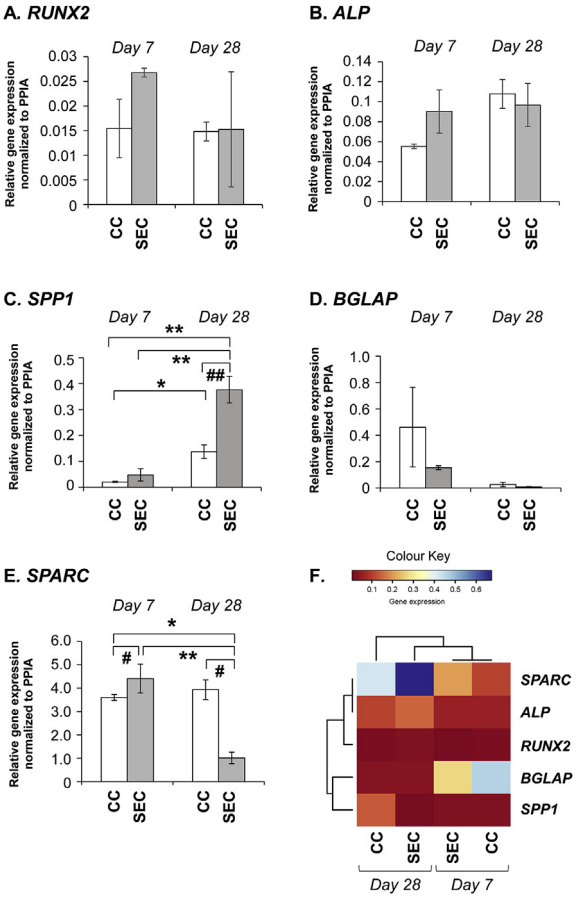

Fig. 9. Relative mRNA expression levels of the osteogenic marker genes alkaline phosphatase (*ALP*), bone gamma-carboxyglutamate (*BGLAP*; osteocalcin), runt-related transcription factor 2 (*RUNX2*), osteonectin (*SPARC*) and osteopontin (*SPP1*) on days 7 and 28 using RT-qPCR. Relative gene expression levels were normalized to PPIA (cyclophilin-A). Asterisks (*) mark significant changes in gene expression level compared to day 7 ($^{*}P < 0.05$; $^{**}P < 0.01$); hash signs (#) mark significant changes compared to the control (CC) within the same measurement day ($^{\#}P < 0.05$; $^{\#\#}P < 0.01$. Data shown are representative of three independent experiments. **F.** Heatmap of the expressed genes in human BM-MSCs cultured with or without coral-derived aragonite scaffold. Different expression levels of the transcripts of the genes related to osteogenesis are shown. The cluster analysis and dendrogram show the difference between the transcripts and the sample groups. Blue and red colours indicate high and low expression levels, respectively. (Values represent the relative expression level of the genes). (For interpretation of the references to colour in this figure legend, the reader is referred to the Web version of this article.)

indicates that the scaffolds did not induce abnormal proliferation pattern of BM-MSCs, suggesting its suitability for *in vivo* clinical applications. The reduced proliferation rate at later time points, e.g. by day 21 (i.e. in more mature osteogenic cell cultures) can also be regarded as a sign of progression in differentiation. Also, the fact that higher numbers of proliferating cells were located in the close proximity of scaffolds as revealed by PCNA immunocytochemistry in 14-day-old cultures indicates the requirement for interaction between the cells and the surface of the scaffold to promote cell division. The observed higher rate of cell proliferation by the scaffold is a sign of its ability to promote osteogenesis from the very beginning of the process, when a rapid proliferation of osteoprogenitors is necessary to establish a higher number of osteoid-secreting late osteoblasts (Javed et al., 2010). Our findings show a similar pattern of cell proliferation to basic fibroblast growth factor (bFGF)-overexpressing bone marrow-derived MSCs reported earlier (Zheng et al., 2011); however, in that study, MSCs seeded onto the coral scaffolds exhibited lower rates of proliferation compared to control. A potential difference that may explain this observation is that MSCs in our study were cultured in osteogenic differentiation medium, whereas Zheng and colleagues cultured the cells in normal DMEM. In a different study, a partially converted, biodegradable coralline hydroxyapatite/calcium carbonate composite comprising of a coralline $CaCO_3$ scaffold enveloped by a thin layer of hydroxyapatite also did not increase the proliferation of hMSCs compared to cells grown on coverslips (Fu et al., 2013). However, when BM-MSCs were seeded onto native coral $CaCO_3$ substrates, a remarkably similar increase in proliferation was reported as determined by [^{3}H]-thymidine incorporation assay (Fricain et al., 1998).

The mechanism underlying the current study may involve surface modification or deposition on the scaffold, resulting in about 2% of the superficial layer mass being changed into calcium phosphate during conversion and/or deposition (see Fig. 6). At the same time, the cells seem to preferentially attach to these deposits and are associated with the formation of spherical calcium phosphate depositions similar in appearance to hydroxyapatite (See Fig. 7).

Taken together, these results clearly demonstrate the osteogenic capacity of the scaffold, in addition to the mitogenic effect on BM-MSCs. The deposition of calcium phosphate on the Agili-C™ scaffold surface supports observations in earlier studies reporting direct osteoconduction by aragonite scaffolds.

5. Conclusions

Under appropriate conditions which favour osteogenesis, these results indicate that the Agili-C™ scaffold can promote the direct adhesion, proliferation and differentiation of human BM-MSCs. The mechanism of ECM formation may involve scaffold surface modification with layering of calcium phosphate deposits supporting osteoconduction (possibly even osteotransduction). As hMSC cultures were maintained in osteogenic media over the entire period of the study, the presence of the scaffolds markedly augmented the osteogenesis-promoting effect of these culturing conditions, enhanced proliferation as well as the osteogenic differentiation of BM-MSCs at both the molecular and histological levels. Based on these results we can conclude that this acellular scaffold is applicable for bone remodelling to promote a faster bone tissue formation in osteochondral lesions or bone fusions and serves as an excellent scaffold for colonisation and osteogenic differentiation of bone marrow derived mesenchymal stem cells.

Declarations

Availability of data and material

Data sharing is not applicable to this article as no datasets were generated or analysed during the current study. Nevertheless, raw data used and/or analysed during the current study are available from the corresponding author on reasonable request.

Competing interests

This paper was written by the authors within the scope of their academic and research positions. Whilst DR, NA and TN are employed by CartiHeal 2009 Ltd, the company had no role in the study design, collection, analysis or interpretation of the data, writing the manuscript, or the decision to submit the paper for publication. The other authors report no conflict of interests.

Funding

CM was supported by the János Bolyai Research Fellowship and the Premium Postdoctoral Research Programme of the Hungarian Academy of Sciences, and a Bridging Fund from the University of Debrecen. CSz-S was supported by the ÚNKP-18-3-III New National Excellence Program of the Ministry of Human Capacities. The funding bodies were not involved in the study design, data collection, analysis and interpretation. The decision to submit the paper for publication was not influenced by any the funding bodies.

Authors' contributions

The manuscript has been read and approved by all named authors, and all authors contributed to the generation of the manuscript as follows. CM, CSz-S, EK, TN, NA, DR and RZ designed the experiments; CM, CSz-S, EK and ZV conducted the research and collected data; all authors participated in data analysis and interpretation, in addition to providing a substantial contribution to discussions. All authors were involved in manuscript writing. All authors reviewed, edited and approved the manuscript before submission. We further confirm that the order of authors listed in the manuscript has been approved by each of the authors and no other persons satisfied the criteria for authorship.

Acknowledgements

The authors are indebted to Mrs Krisztina Biróné Barna for excellent and skilful technical assistance. We are grateful to Dr Zoltan Varga (Department of Biophysics, Faculty of Medicine, University of Debrecen) for his assistance in data analysis. Real-time qPCR measurements were performed by UD-GenoMed Medical Genomic Technologies Ltd, Debrecen, Hungary.

References

Al-Salihi, K.A., Samsudin, A.R., 2004. Bone marrow mesenchymal stem cells differentiation and proliferation on the surface of coral implant. Med. J. Malays. 59 (Suppl. B), 45–46.
Albrektsson, T., Johansson, C., 2001. Osteoinduction, osteoconduction and osseointegration. Eur. Spine J. 10 (Suppl. 2), S96–S101.
Beck, G.R., Zerler, B., Moran, E., 2000. Phosphate is a specific signal for induction of osteopontin gene expression. Proc. Natl. Acad. Sci. Unit. States Am. 97 (15), 8352–8357.
Birk, R.Z., Abramovitch-Gottlib, L., Margalit, I., Aviv, M., Forti, E., Geresh, S., Vago, R., 2006. Conversion of adipogenic to osteogenic phenotype using crystalline porous biomatrices of marine origin. Tissue Eng. 12 (1), 21–31.
Blom, E.J., Klein-Nulend, J., Yin, L., van Waas, M.A., Burger, E.H., 2001. Transforming growth factor-beta1 incorporated in calcium phosphate cement stimulates osteotransductivity in rat calvarial bone defects. Clin. Oral Implant. Res. 12 (6), 609–616.
Bowland, P., Ingham, E., Jennings, L., Fisher, J., 2015. Review of the biomechanics and biotribology of osteochondral grafts used for surgical interventions in the knee. Proc. IME H J. Eng. Med. 229 (12), 879–888.
Chiroff, R.T., White, E.W., Weber, J.N., Roy, D.M., 1975. Tissue ingrowth of replamineform implants. J. Biomed. Mater. Res. 9 (4), 29–45.
Choi, M.H., Noh, W.C., Park, J.W., Lee, J.M., Suh, J.Y., 2011. Gene expression pattern during osteogenic differentiation of human periodontal ligament cells in vitro. J. Periodontal Implant Sci. 41 (4), 167–175.
Chubinskaya, S., Di Matteo, B., Lovato, L., Iacono, F., Robinson, D., Kon, E., 2018. Agili-C implant promotes the regenerative capacity of articular cartilage defects in an ex vivo model. Knee Surg. Sport. Traumatol. Arthrosc.
Ciocca, L., Lesci, I.G., Mezini, O., Parrilli, A., Ragazzini, S., Rinnovati, R., Romagnoli, N., Roveri, N., Scotti, R., 2017. Customized hybrid biomimetic hydroxyapatite scaffold for bone tissue regeneration. J. Biomed. Mater. Res. B Appl. Biomater. 105 (4), 723–734.
Conserva, E., Foschi, F., Cancedda, R., Mastrogiacomo, M., 2013. In vitro and in vivo osteoinductive and osteoconductive properties of a synthetic bone substitute. Int. J. Oral Maxillofac. Implant. 28 (6), e432–439.
Demers, C., Hamdy, C.R., Corsi, K., Chellat, F., Tabrizian, M., Yahia, L., 2002. Natural coral exoskeleton as a bone graft substitute: a review. Bio Med. Mater. Eng. 12 (1), 15–35.
Dominici, M., Le Blanc, K., Mueller, I., Slaper-Cortenbach, I., Marini, F., Krause, D., Deans, R., Keating, A., Prockop, D., Horwitz, E., 2006. Minimal criteria for defining multipotent mesenchymal stromal cells. The International Society for Cellular Therapy position statement. Cytotherapy 8 (4), 315–317.
Driessens, F.C., Planell, J.A., Boltong, M.G., Khairoun, I., Ginebra, M.P., 1998. Osteotransductive bone cements. Proc. Inst. Mech. Eng. H 212 (6), 427–435.
Ducy, P., Zhang, R., Geoffroy, V., Ridall, A.L., Karsenty, G., 1997. Osf2/Cbfa1: a transcriptional activator of osteoblast differentiation. Cell 89 (5), 747–754.
Fedde, K.N., 1992. Human osteosarcoma cells spontaneously release matrix-vesicle-like structures with the capacity to mineralize. Bone Miner. 17 (2), 145–151.
Fermor, H.L., Russell, S.L., Williams, S., Fisher, J., Ingham, E., 2015. Development and characterisation of a decellularised bovine osteochondral biomaterial for cartilage repair. J. Mater. Sci. Mater. Med. 26 (5), 1–11.
Figueroa, R.J., Koch, T.G., Betts, D.H., 2011. Osteogenic differentiation of equine cord blood multipotent mesenchymal stromal cells within coralline hydroxyapatite scaffolds in vitro. Vet. Comp. Orthop. Traumatol. 24 (5), 354–362.
Foo, L.H., Suzina, A., Azlina, A., Kannan, T., 2008. Gene expression analysis of osteoblasts seeded in coral scaffold. J. Biomed. Mater. Res. A 87 (1), 215–221.
Fricain, J., Bareille, R., Ulysse, F., Dupuy, B., Amedee, J., 1998. Evaluation of proliferation and protein expression of human bone marrow cells cultured on coral crystallized in the aragonite or calcite form. J. Biomed. Mater. Res. 42 (1), 96–102.
Fu, K., Xu, Q., Czernuszka, J., Triffitt, J.T., Xia, Z., 2013. Characterization of a biodegradable coralline hydroxyapatite/calcium carbonate composite and its clinical implementation. Biomed. Mater. 8 (6), 065007.
Guillemin, G., Patat, J.L., Fournie, J., Chetail, M., 1987. The use of coral as a bone graft substitute. J. Biomed. Mater. Res. 21 (5), 557–567.
Harris, C.T., Cooper, L.F., 2004. Comparison of bone graft matrices for human mesenchymal stem cell-directed osteogenesis. J. Biomed. Mater. Res. A 68 (4), 747–755.
Javed, A., Chen, H., Ghori, F.Y., 2010. Genetic and transcriptional control of bone formation. Oral Maxillofac. Surg. Clin. 22 (3), 283–293.
Kazemzadeh-Narbat, M., Kindrachuk, J., Duan, K., Jenssen, H., Hancock, R.E., Wang, R., 2010. Antimicrobial peptides on calcium phosphate-coated titanium for the prevention of implant-associated infections. Biomaterials 31 (36), 9519–9526.
Kon, E., Drobnic, M., Davidson, P.A., Levy, A., Zaslav, K., Robinson, D., 2014a. Chronic posttraumatic cartilage lesion of the knee treated with an acellular osteochondral-regenerating implant: case history with rehabilitation guidelines. J. Sport Rehabil. 23 (3), 270–275.
Kon, E., Filardo, G., Robinson, D., Eisman, J.A., Levy, A., Zaslav, K., Shani, J., Altschuler, N., 2014b. Osteochondral regeneration using a novel aragonite-hyaluronate bi-phasic scaffold in a goat model. Knee Surg. Sport. Traumatol. Arthrosc. 22 (6), 1452–1464.
Kon, E., Filardo, G., Shani, J., Altschuler, N., Levy, A., Zaslav, K., Eisman, J.E., Robinson, D., 2015. Osteochondral regeneration with a novel aragonite-hyaluronate biphasic scaffold: up to 12-month follow-up study in a goat model. J. Orthop. Surg. Res. 10 (1), 1–17.

Kon, E., Robinson, D., Verdonk, P., Drobnic, M., Patrascu, J.M., Dulic, O., Gavrilovic, G., Filardo, G., 2016. A novel aragonite-based scaffold for osteochondral regeneration: early experience on human implants and technical developments. Injury 47 (Suppl. 6), S27–S32.

Kulterer, B., Friedl, G., Jandrositz, A., Sanchez-Cabo, F., Prokesch, A., Paar, C., Scheideler, M., Windhager, R., Preisegger, K.-H., Trajanoski, Z., 2007. Gene expression profiling of human mesenchymal stem cells derived from bone marrow during expansion and osteoblast differentiation. BMC Genomics 8 (1), 70.

Marsell, R., Einhorn, T.A., 2011. The biology of fracture healing. Injury 42 (6), 551–555.

Mesallati, T., Sheehy, E., Vinardell, T., Buckley, C., Kelly, D., 2015. Tissue engineering scaled-up, anatomically shaped osteochondral constructs for joint resurfacing. Eur. Cells Mater. 30, 163–186.

Mygind, T., Stiehler, M., Baatrup, A., Li, H., Zou, X., Flyvbjerg, A., Kassem, M., Bunger, C., 2007. Mesenchymal stem cell ingrowth and differentiation on coralline hydroxyapatite scaffolds. Biomaterials 28 (6), 1036–1047.

Niu, C.C., Lin, S.S., Chen, W.J., Liu, S.J., Chen, L.H., Yang, C.Y., Wang, C.J., Yuan, L.J., Chen, P.H., Cheng, H.Y., 2015. Benefits of biphasic calcium phosphate hybrid scaffold-driven osteogenic differentiation of mesenchymal stem cells through upregulated leptin receptor expression. J. Orthop. Surg. Res. 10, 111.

Ohgushi, H., Okumura, M., Yoshikawa, T., Inboue, K., Senpuku, N., Tamai, S., Shors, E.C., 1992. Bone formation processin porous calcium carbonate and hydroxyapatite. J. Biomed. Mater. Res. 26 (7), 885–895.

Olah, L., Borbas, L., 2008. Properties of calcium carbonate-containing composite scaffolds. Acta Bioeng. Biomech. 10 (1), 61.

Pittenger, M.F., Mackay, A.M., Beck, S.C., Jaiswal, R.K., Douglas, R., Mosca, J.D., Moorman, M.A., Simonetti, D.W., Craig, S., Marshak, D.R., 1999. Multilineage potential of adult human mesenchymal stem cells. Science 284 (5411), 143–147.

Polini, A., Wang, J., Bai, H., Zhu, Y., Tomsia, A.P., Mao, C., 2014. Stable biofunctionalization of hydroxyapatite (HA) surfaces by HA-binding/osteogenic modular peptides for inducing osteogenic differentiation of mesenchymal stem cells. Biomater. Sci. 2, 1779–1786.

Puvaneswary, S., Raghavendran, H.R.B., Ibrahim, N.S., Murali, M.R., Merican, A.M., Kamarul, T., 2013. A comparative study on morphochemical properties and osteogenic cell differentiation within bone graft and coral graft culture systems. Int. J. Med. Sci. 10 (12), 1608.

Ram, V.S., Parthiban, U.S., Mithradas, N., Prabhakar, R., 2015. Bonebiomarkers in periodontal disease: a review article. J. Clin. Diagn. Res.: J. Clin. Diagn. Res. 9 (1), ZE07.

Ripamonti, U., 2017. Biomimetic functionalized surfaces and the induction of bone formation. Tissue Eng. 23 (21–22), 1197–1209.

Ripamonti, U., Crooks, J., Khoali, L., Roden, L., 2009. The induction of bone formation by coral-derived calcium carbonate/hydroxyapatite constructs. Biomaterials 30 (7), 1428–1439.

Scaglione, S., Ilengo, C., Fato, M., Quarto, R., 2008. Hydroxyapatite-coated polycaprolacton wide mesh as a model of open structure for bone regeneration. Tissue Eng. 15 (1), 155–163.

Scott, W.N., 2011. Insall & Scott Surgery of the Knee. W. N. Scott. Churchill Livingstone.

Sodek, J., Ganss, B., McKee, M., 2000. Osteopontin. Crit. Rev. Oral Biol. Med. 11 (3), 279–303.

Thorpe, A.A., Creasey, S., Sammon, C., Le Maitre, C.L., 2016. Hydroxyapatite nanoparticle injectable hydrogel scaffold to support osteogenic differentiation of human mesenchymal stem cells. Eur. Cells Mater. 32, 1–23.

Wang, J., Yang, M., Zhu, Y., Wang, L., Tomsia, A.P., Mao, C., 2014. Phage nanofibers induce vascularized osteogenesis in 3D printed bone scaffolds. Adv. Mater. 26 (29), 4961–4966.

Wu, H., Whitfield, T.W., Gordon, J.A., Dobson, J.R., Tai, P.W., van Wijnen, A.J., Stein, J.L., Stein, G.S., Lian, J.B., 2014. Genomic occupancy of Runx2 with global expression profiling identifies a novel dimension to control of osteoblastogenesis. Genome Biol. 15 (3), R52.

Wu, Y.C., Lee, T.M., Chiu, K.H., Shaw, S.Y., Yang, C.Y., 2009. A comparative study of the physical and mechanical properties of three natural corals based on the criteria for bone-tissue engineering scaffolds. J. Mater. Sci. Mater. Med. 20 (6), 1273–1280.

Yang, M., Zhou, G., Castano-Izquierdo, H., Zhu, Y., Mao, C., 2015a. Biomineralization of natural collagenous nanofibrous membranes and their potential use in bone tissue engineering. J. Biomed. Nanotechnol. 11 (3), 447–456.

Yang, M., Zhou, G., Shuai, Y., Wang, J., Zhu, L., Mao, C., 2015b. Ca(2+)-induced self-assembly of Bombyx mori silk sericin into a nanofibrous network-like protein matrix for directing controlled nucleation of hydroxylapatite nano-needles. J. Mater. Chem. B 3 (12), 2455–2462.

Zheng, Y.H., Su, K., Jian, Y.T., Kuang, S.J., Zhang, Z.G., 2011. Basic fibroblast growth factor enhances osteogenic and chondrogenic differentiation of human bone marrow mesenchymal stem cells in coral scaffold constructs. J. Tissue Eng. Regenerat. Med. 5 (7), 540–550.

Zoch, M.L., Clemens, T.L., Riddle, R.C., 2016. New insights into the biology of osteocalcin. Bone 82, 42–49.